Single-Particle Spectroscopic Measurements of Fluorescent Graphene Quantum Dots

Qinfeng Xu,[†,§] Qi Zhou,[†] Zheng Hua,[†] Qi Xue,[‡] Chunfeng Zhang,[†] Xiaoyong Wang,[*,†] Dengyu Pan,[*,‡] and Min Xiao[*,†,⊥]

[†]National Laboratory of Solid State Microstructures and School of Physics, Nanjing University, Nanjing 210093, China, [‡]Institute of Nanochemistry and Nanobiology, Shanghai University, Shanghai 201800, China, [§]Department of Physics and Optoelectronic Engineering, Ludong University, Yantai 264025, China, and [⊥]Department of Physics, University of Arkansas, Fayetteville, Arkansas 72701, United States

ABSTRACT We have performed the first single-particle spectroscopic measurements on individual graphene quantum dots (GQDs) and revealed several intriguing fluorescent phenomena that are otherwise hidden in the optical studies of ensemble GQDs. First, despite noticeable differences in the size and the number of layers from particle to particle, all of the GQDs studied possess almost the same spectral lineshapes and peak positions. Second, GQDs with more layers are normally brighter emitters but are associated with shorter fluorescent lifetimes. Third, the fluorescent spectrum of GQDs was red-shifted upon being aged in air, possibly due to the water desorption effect. Finally, the missing emission of single photons and stable fluorescence without any intermittent behavior were observed from individual GQDs.

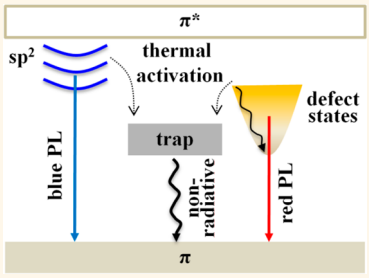

KEYWORDS: graphene oxide · graphene quantum dots · photoluminescence · single-particle · time-resolved

Graphene oxide (GO) can be described as a two-dimensional (2D) network of graphite containing nanometer-sized regions of sp^2-hybridized carbon atoms dispersed within a carbon−oxygen sp^3 matrix.[1,2] In contrast to the zero-gap semiconductor of pristine graphene that gains its fame with superior electrical transport properties,[3] the energy-gap opening in GO due to the introduction of oxygen functional groups makes it attractive for various optical applications, such as in photocatalysis,[4] solar cells,[5] light-emitting diodes,[6] and biological imaging.[7] The GO fluorescence has been reported to cover a broad wavelength range from ultraviolet to visible to near-infrared, with the underlying mechanisms now being actively pursued in the research community.[8−14] Owning to the continuous improvement on the synthesis strategies, the past several years have seen the emergence of a handful of techniques[15] for making miniaturized versions of GO sheets, generally called graphene quantum dots (GQDs), with the sizes ranging from several to tens of nanometers. These single- or few-layer GQDs can potentially provide an alternative yet succinct view of the GO optical properties since their sp^2 domains decorated with oxygen functional groups might be the main fluorescence contributing units before being isolated out of the GO sheet.[8,9,11,13,14] Unfortunately, all of the previous optical studies of GQDs reported so far were performed exclusively on the ensemble level,[15−27] only yielding averaged fluorescent characteristics that are not quite different from those demonstrated by their GO sheet counterparts.

In this report, we have performed the first single-particle spectroscopic measurements on individual GQDs and revealed several intriguing fluorescent phenomena that are otherwise hidden in the optical studies of GO sheets and GQD ensembles. First, despite noticeable differences in the size and the number of layers from particle to particle, all of the GQDs studied possess almost the same spectral lineshapes and peak positions. Second, GQDs with more layers are normally brighter emitters but are associated with shorter fluorescent lifetimes. Third, the fluorescent spectrum of GQDs was red-shifted upon being aged in air,

* Address correspondence to wxiaoyong@nju.edu.cn, dypan617@shu.edu.cn, mxiao@uark.edu.

Received for review June 30, 2013 and accepted November 19, 2013.

Published online November 19, 2013
10.1021/nn4053342

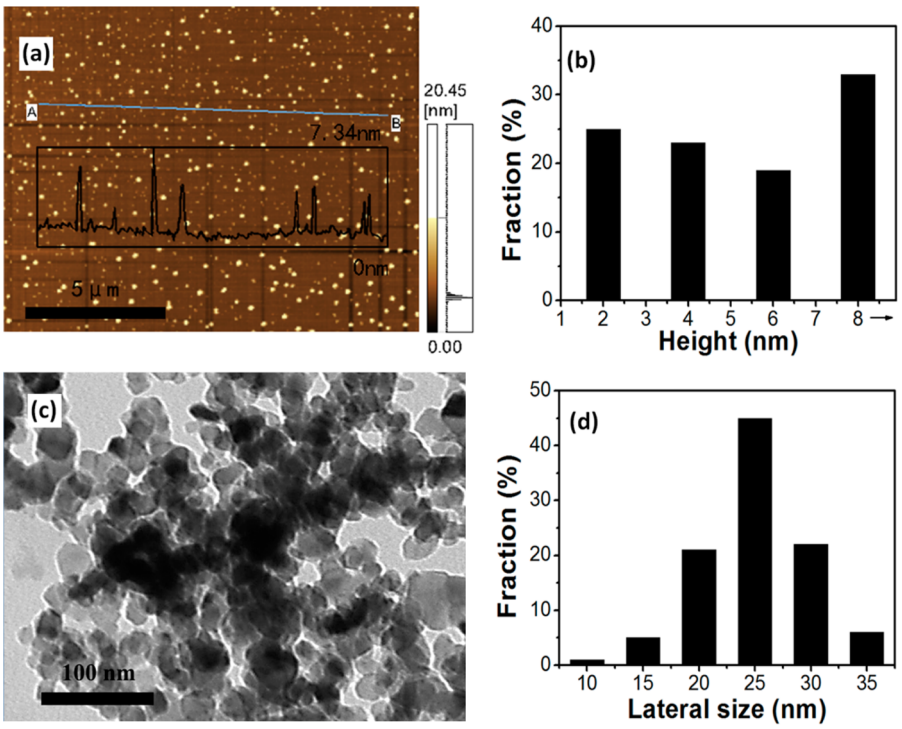

Figure 1. (a) AFM image of GQDs. The inset shows a height profile of the GQDs measured along the solid line (from A to B) in the AFM image. (b) The height distributions of GQDs obtained from the AFM image. (c) TEM image of GQDs. (d) The size distributions of GQDs obtained from the TEM image.

possibly due to the water desorption effect. Finally, the missing emission of single photons and stable fluorescence without any intermittent behavior were observed from individual GQDs.

RESULTS AND DISCUSSION

The GQDs were prepared by a hydrothermal cutting method[16] without further dialysis. The atomic force microscopy (AFM) image (Figure 1a) of the hydrophilic GQDs deposited on a mica substrate exhibits a height distribution within ~2−8 nm (Figure 1b), implying that most of the GQDs are composed of few-layer carbon sheets. The lateral sizes of GQDs were determined by the transmission electron microscopy (TEM) measurement (Figure 1c) to be in the range ~10−35 nm (Figure 1d). As reported previously by us[16] and is commonly encountered in both GO sheets[13,14] and GQDs,[15,18,20,21,23] their photoluminescence (PL) bands shift to the red side with the increasing excitation wavelengths. In Figure 2a, we plot two representative PL spectra of the ensemble GQDs excited at the laser wavelengths of 266 and 400 nm with the corresponding emission peaks centered at ~460 nm and ~520 nm, respectively. These two peak positions fall within a wavelength range whose fluorescent origins have been classified into two main categories for both GO sheets and GQDs. As schematically shown in Figure 3, photoexcited electrons through the $\pi-\pi^*$ transitions were proposed to relax into either the sp^2 energy levels or the defect states, giving rise to the blue or red PL, respectively.[11,24,28] The former emission might bear the discrete feature due to quantum confinement of electrons inside the sp^2 carbon domains.[9−11,17,19,20] The latter emission, which is related to the oxygen functional groups decorating the intrinsic sp^2 domains at the edges and/or on the basal planes,[11−13,21,22] could possess broad absorption and emission bands within the $\pi-\pi^*$ gap.[11,21] This naturally explains the excitation wavelength dependence of the GO and GQD PL since different defect states are selected in this case to yield a specific spectral pattern (Figure 3).

In Figure 2b, we present the PL decay curves measured for the two PL bands in Figure 2a, and they can be both fitted well using a biexponential function of $I(t) = A_1 e^{-t/\tau_1} + A_2 e^{-t/\tau_2}$. Here, A_1 (A_2) and τ_1 (τ_2) are the percentage contribution and value of the faster (slower) lifetime component, respectively, from which we can define a weighted-average lifetime of $\tau_{average} = A_1\tau_1 + A_2\tau_2$.[29] Overall, the PL decay is faster for the 460 nm band ($\tau_{average} = 0.84 \pm 0.01$ ns) excited at 266 nm than that measured for the 520 nm band ($\tau_{average} = 1.29 \pm 0.02$ ns) excited at 400 nm, which can be used as a plausible proof to show that these two bands do have different electronic origins.[11,24] However, as can be conceived from Figure 3, electrons of the higher-lying defect states are more likely to decay into the lower-lying defect states and nonemissive traps in addition to their radiative recombination. Then the lifetime discrepancy observed in Figure 2b can be alternatively explained without involving the sp^2-related states if we

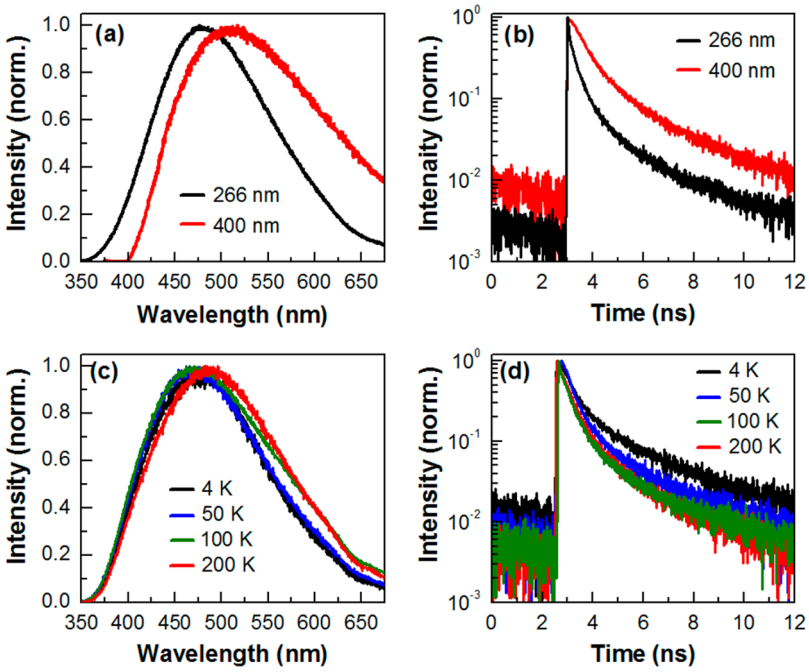

Figure 2. (a) PL spectra and (b) PL decay curves of ensemble GQDs measured at room temperature with the pulsed laser excitations at 266 and 400 nm, respectively. (c) PL spectra and (d) PL decay curves of ensemble GQDs measured at four representative temperatures with the pulsed laser excitation at 266 nm. In b, the biexponential fitting parameters (A_1, A_2; τ_1, τ_2; $\tau_{average}$) are (82%, 18%; 0.63 ns, 1.79 ns; 0.84 $\pm$ 0.01 ns) for the 266 nm excitation and (84%, 16%; 0.73 ns, 4.26 ns; 1.29 $\pm$ 0.02 ns) for the 400 nm excitation, respectively. In d, the biexponential fitting parameters (A_1, A_2; τ_1, τ_2; $\tau_{average}$) are (83%, 17%; 0.54 ns, 3.05 ns; 0.97 $\pm$ 0.01 ns) at 4 K, (80%, 20%; 0.41 ns, 2.24 ns; 0.78 $\pm$ 0.02 ns) at 50 K, (79%, 21%; 0.44 ns, 1.83 ns; 0.73 $\pm$ 0.02 ns) at 100 K, and (78%, 22%; 0.48 ns, 1.79 ns; 0.77 $\pm$ 0.02 ns) at 200 K, respectively.

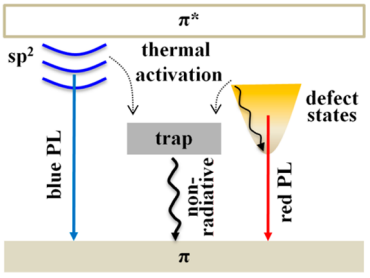

Figure 3. Energy level structures to explain the optical behaviors of photoexcited electrons in both GO sheets and GQDs, including their radiative recombination from discrete sp^2-related states and continuous defect states, thermally activated decay into nonradiative traps, and nonradiative relaxation from higher- to lower-lying defect states.

assume that electrons of lower-lying defect states sampled at longer excitation wavelengths suffer less from the nonradiative decay, thus leading to an apparent increase of the PL decay lifetime. This scenario is similar to what has been observed in semiconductor CdSe and PbSe QDs that photoexcited carriers in the higher energy states suffer more from relaxation into nonradiative surface traps,[30,31] leading to the well-known charged-exciton issue in their PL blinking[32] and carrier multiplication[33] studies. We next excited the ensemble GQDs with the 266 nm laser at variable temperatures, only to see that the PL peak shifted slightly to the blue side with no detectable spectral narrowing at low temperatures (Figure 2c). Meanwhile, their PL decay dynamics get a little expedited with the increasing temperature (Figure 2d), possibly due to the increased probability for the sp^2 and/or defect state electrons to be thermally activated into nonradiative traps (Figure 3) that might originate from imperfect surface/edge passivations.[21,26,27]

After the PL characterizations in Figure 2, showing that the optical properties of GQDs studied here on the ensemble level are not any different from those of other GQD and GO samples reported in the literature, we next turned to single-particle spectroscopic measurements to probe if there is still any hidden fluorescent information that can be revealed from individual GQDs. The spatial and spectral PL images for a number of individual GQDs excited at 400 nm are shown in Figure 4a and b, respectively, together with the PL spectra in Figure 3c for four selected individual GQDs excited at 266 nm. Due to the hydrophilic nature of the silica coverslips used in our experiment, the deposited GQDs are well-dispersed without any clustering effect, as evidenced by the diffraction-limited image spots shown in Figure 4a. It can be clearly seen from Figure 4b and c that, despite a relatively large size distribution of the individual GQDs (Figure 1d), their PL spectra are basically the same in terms of the spectral peak positions and lineshapes. This kind of size-independent PL characteristics, observed previously in ensemble GQDs,[21] is confirmed here again on the individual level. Similar to the ensemble case in Figure 2c, we observed

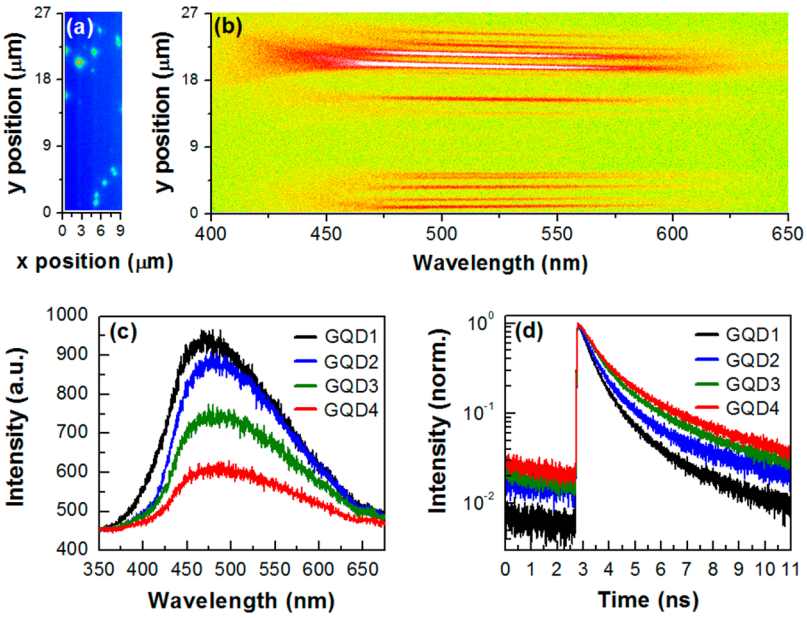

Figure 4. (a) Spatial and (b) spectral PL images of individual GQDs measured at room temperature with the pulsed laser excitation at 400 nm. (c) PL spectra and (d) PL decay curves of four representative GQDs measured at room temperature with the pulsed laser excitation at 266 nm. In d, the biexponential fitting parameters (A_1, A_2; τ_1, τ_2; $\tau_{average}$) are (81%, 19%; 0.49 ns, 1.81 ns; 0.74 ± 0.02 ns) for GQD1, (77%, 23%; 0.69 ns, 2.64 ns; 1.13 ± 0.02 ns) for GQD2, (75%, 25%; 0.71 ns, 3.33 ns; 1.37 ± 0.02 ns) for GQD3, and (71%, 29%; 0.73 ns, 3.54 ns; 1.54 ± 0.03 ns) for GQD4, respectively.

from the temperature-dependent measurements (not shown) that there were almost no changes in the PL peak positions and lineshapes of individual GQDs.

The spatial PL image of Figure 4a contains both brighter and dimer GQDs, whose fluorescence intensity difference is further emphasized in Figure 4c. We speculate that brighter GQDs are composed of more layers of sp^2 domains (Figure 1a) based on the time-resolved measurements in Figure 4d, which shows that they are correlated with shorter PL decay lifetimes. For single-layer GQDs, their PL decay process consists of both radiative electron−hole recombination and nonradiative carrier relaxation into other emissive or nonemissive states (Figure 3). When multiple layers of sp^2 domains are stacked together, one additional channel for the nonradiative decay of carriers would be opened due to possible interactions between neighboring layers,[10] which explains the shortening of PL decay lifetime in brighter or multiple-layer GQDs observed in Figure 4d. On the other hand, the increasing number of absorption and emission units in a multiple-layer GQD favors an enhancement of its PL intensity, which should be larger than that of a single-layer GQD but smaller than would be combined from all the composing layers without nonradiative interactions. Since the adjacent layers of GQDs are commonly isolated by oxygen functional groups and water molecules[20,21] to prevent any direct migration of photoexcited carriers, their nonradiative interactions might be realized through the Förster-type energy transfer process[30] that has been previously invoked to explain the fluorescence quenching effect caused by GO sheets.[1]

The GQDs studied here were prepared hydrothermally and have shown hours of stable emission in solution.[16,34] Thanks to the sensitivity of the single-particle spectroscopic measurement, we were able to resolve red-shifted optical emissions from individual GQDs in their aging process. This can be clearly seen in Figure 5a from the two PL spectra of a representative GQD, which were obtained with the 266 nm excitation right after it was deposited onto the coverslip from solution and when it had endured an overnight exposure to the ambient environment, respectively. Meanwhile, the red-shifted PL was accompanied by an elongated PL decay lifetime of $\tau_{average}$ = 0.96 ± 0.02 ns in the aged GQD as compared to that of $\tau_{average}$ = 0.87 ± 0.02 ns measured when it was still fresh (Figure 5b). One possible origin of this red-shifted PL is that the GQDs were oxidized in their aging process with the addition of oxygen-containing function groups, which would form more lower-lying defect states emitting on the red side of the PL spectrum (Figure 2a) with a relatively longer radiative lifetime (Figure 2b). However, the X-ray photoelectron spectroscopy (XPS) measurements of ensemble GQDs demonstrated that it was the C−C peak whose percentage contribution to the integrated area of the C 1s spectrum increased in the aging process (see Supporting Information, Figure S1). To further exclude the contribution of oxidation to the red-shifted PL, we placed a freshly made film of individual GQDs inside a vacuum chamber. As representatively shown in Figure 5c, after about one day of vacuum pumping, the red-shifted PL could still be observed from an

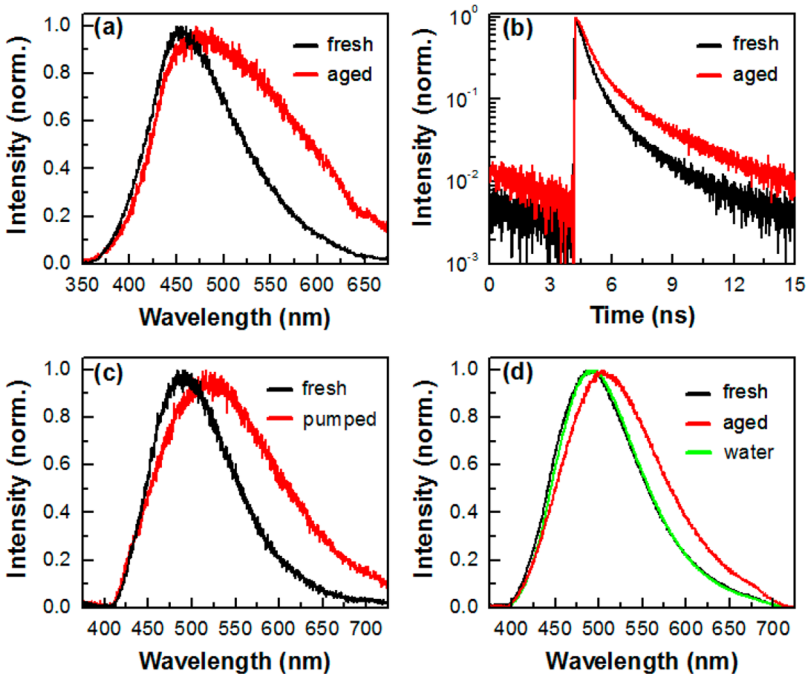

Figure 5. (a) PL spectra and (b) PL decay curves of a representative GQD measured during the fresh and aged stages, respectively. These measurements were performed at room temperature with the pulsed laser excitation at 266 nm. In b, the biexponential fitting parameters (A_1, A_2; τ_1, τ_2; $\tau_{average}$) are (79%, 21%; 0.50 ns, 2.24 ns; 0.87 ± 0.02 ns) for the fresh GQD and (84%, 16%; 0.59 ns, 2.93 ns; 0.96 ± 0.02 ns) for the aged GQD, respectively. (c) PL spectra of an individual GQD excited at 400 nm on a freshly made film and after the film has been placed inside a vacuum chamber continuously pumped for about one day. (d) PL spectra of an individual GQD excited at 400 nm on a freshly made film (black), after the film had been exposed in the ambient environment for about 10 h (red), and after water was added to the aged sample (green).

individual GQD excited at 400 nm, although there should be no oxygen molecules around.

Moreover, the above vacuum experiment has also implied that the red-shifted PL might be caused by water desorption from the GQD sheets. To verify this, we did one additional experiment to first observe that the PL spectrum of an individual GQD excited at 400 nm on a freshly made film shifted to the red side after it had been exposed in the air for about 10 h (Figure 5d). Then after a small amount of water was sprayed onto the film, the PL peak of this GQD shifted back to its original position, thus unambiguously confirming that the red-shifted PL of aged GQDs should be a direct consequence of water desorption. This reversible PL shift of GQDs upon addition/removal of water molecules should find an immediate application in environmental sensing devices and would surely stimulate extensive theoretical modellings on its exact electronic origin. For now, a possible explanation is that the desorption of water molecules from between neighboring GQD sheets would make a better $\pi-\pi$ stacking, which has been shown previously to cause the red-shifted PL in some organic/inorganic building molecules.[35] This kind of enhanced $\pi-\pi$ stacking of GQD sheets might greatly increase the mobility of charge carriers[35] to extend their spatial confinement from two to three dimensions, leading to the red-shifted PL, and to reduce the overlap of electron and hole wave functions, thus elongating the radiative lifetime of excitons.

Finally, with the 405 nm pulsed laser excitation at a repetition rate of 10 MHz, we performed single photon antibunching and PL intensity *versus* time trace measurements for both single CdSe QDs and individual GQDs. In Figure 6a, we plot the second-order intensity correlation function $g^{(2)}(t)$ measured for a representative CdSe QD, which gives the probability of detecting two consecutively emitted photons at variable time delays.[36,37] If an excitation pulse has already triggered a photon from a single CdSe QD, no other photons would be emitted within the pulse duration due to the quantized nature of its energy level structures,[38] thus leading to a missing peak, or a vanishing $g^{(2)}(t)$ probability, at zero time delay in Figure 6a. On the other hand, the probability of registering a second photon would be high with the arrivals of other excitation pulses, so that one could observe all of those peaks at the integer multiples of the pulse separation of ~100 ns. We then performed the same $g^{(2)}(t)$ measurements with ~10 single- or few-layer individual GQDs, corresponding to those dimer spots in Figure 4a. As shown in Figure 6b for a representative GQD, the appearance of a central peak at zero time delay unambiguously proves that multiple photons are emitted with the excitation of a single laser pulse and it cannot serve as a quantized single photon emitter. We next investigated if an individual GQD can be treated as a single molecular emitter, whose fluorescence should universally possess an intensity intermittency,[32,37,39] which is representatively

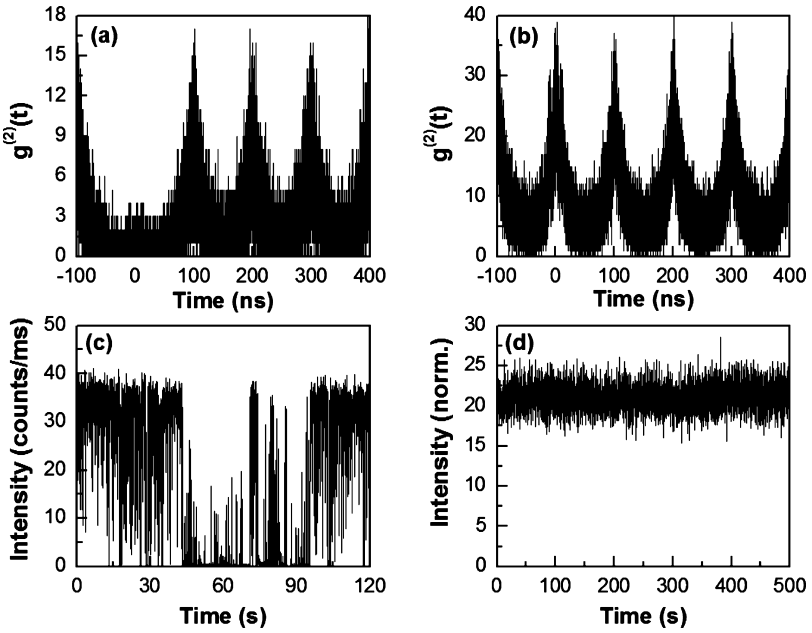

Figure 6. Second-order photon correlation functions measured for (a) a single CdSe QD and (b) an individual GQD. PL intensity *versus* time traces measured for (c) a single CdSe QD and (d) an individual GQD. All of the measurements were performed at room temperature with a 10 MHz, pulsed 405 nm laser.

shown in Figure 6c for a single CdSe QD. In contrast, all of the individual GQDs studied showed stable fluorescence over the measurement time, as can be clearly seen in Figure 6d from the PL intensity *versus* time trace of a representative GQD. This kind of stable fluorescence, which is free of PL intermittency and bleaching effects, highlights the great advantage of individual GQDs over traditional organic dyes and semiconductor QDs as nanometer-sized fluorescent chromophores.

The dramatically different optical behaviors between single CdSe QDs and individual GQDs might point to the fact that optical emissions of GQDs are mainly from continuous defect states. Then a full understanding of the formation mechanisms of these defect states and a judicious control of their fluorescent characteristics in future work would benefit a variety of applications for both GO sheets and GQDs,[1,2,15,28] especially those specific to GQDs in biological labeling, imaging, and functional nanodevices.[18,23,26] On the other hand, this discrepancy might reflect an alternative scenario where the 2D sheet of a single-layer GQD can be still divided into even smaller sp^2 domains separated by oxygen functional groups, so that the single-particle spectroscopic measurement is in fact conducted on a fluorescent ensemble. This is supported by previous scanning tunneling microscopy[40,41] and TEM[42] measurements with GO sheets that have revealed the existence of nanometer-sized sp^2 clusters (~2−3 nm), whose isolated form of ultrasmall (~1.65 nm) GQDs was recently reported to emit ultraviolet light.[21] In this case, we believe that more exciting breakthroughs would be made if quantized optical emissions from the real sp^2 domains can be finally brought into play to greatly boom the fundamental research of GQDs in the context of quantum information science applications.

CONCLUSIONS

To summarize, we have studied individual GQDs with a single-particle spectroscopic technique, which has provided a more informative description of their optical properties than the ensemble approach. Although the PL lineshapes and peak positions of individual GQDs are not size-dependent, their PL intensities and lifetimes are strongly affected by the number of composing layers. Upon being aged in the ambient atmosphere, nearly all of the individual GQDs measured showed some degree of red-shifted PL, which could be recovered back with the addition of water molecules. Finally, no single photon emission was detected from individual GQDs, but their stable fluorescence, which is free of the PL intermittency and bleaching effects, may indicate their great advantage over traditional organic dyes and semiconductor QDs as nanometer-sized fluorescent chromophores.

EXPERIMENTAL SECTION

Sample Preparation. The GQDs were prepared by a hydrothermal cutting method[16] without further dialysis. As a reference for the single-particle spectroscopic measurement, we also studied commercial CdSe QDs with the emission peak wavelength at ~655 nm (Qdot 655 from Invitrogen). One drop of the sample solution with an appropriate density of GQDs or CdSe QDs dispersed in deionized water was spin-cast onto a

fused silica coverslip to form a solid film for the optical characterizations.

Optical Characterization. All of the optical measurements were performed at room temperature unless otherwise specified in the text. The 800 nm output of a 76 MHz, picosecond Ti:sapphire laser was used to get the excitation wavelengths of 400 and 266 nm from the second and third harmonic generation processes, respectively. The 266 or 400 nm laser beam with a power density of ~100 W/cm^2 and at an incident angle of ~45° relative to the normal direction was focused onto the GQD sample films at either room temperature or low temperatures with a helium flow cryostat. The fluorescence signal was collected vertically from the film surface by a 60× microscope objective and sent through a 0.5 m spectrometer to a charge-coupled-device camera for spatial and spectral PL characterizations or to an avalanche photodiode for the PL decay measurements using a time-correlated single-photon counting system with a time resolution of ~250 ps. Since the PL decay lifetimes of GQDs studied here are on the time scale of several nanosconds, we mainly used a laser repetition rate of ~76 MHz for all of the PL decay measurements. We have also employed smaller laser repetition rates for the time-resolved measurements, and the weighted-average lifetimes of GQDs are basically the same within the experimental error (see Supporting Information, Figure S2). For the PL intensity *versus* time trace and photon antibunching measurements, the GQD or CdSe QD sample was loaded to a scanning confocal microscope equipped with a piezo scanner with a spatial resolution of ~100 nm. The 405 nm beam of a 10 MHz, picosecond diode laser was focused onto the sample surface at the power density of ~100 W/cm^2 with a 100× immersion-oil objective. The single-particle fluorescence signal was collected by the same objective and sent through a beamsplitter tube to two avalanche photodiodes in a Hanbury Brown−Twiss configuration.

Conflict of Interest: The authors declare no competing financial interest.

Acknowledgment. The authors would like to thank the National Basic Research Program of China (nos. 2012CB921801 and 2011CBA00205), the National Natural Science Foundation of China (nos. 91021013, 11274161, 11021403, 61307067, 11174194, and 91233102), the New Century Excellent Talents program (NCET-11-0238), Jiangsu Provincial Funds for Distinguished Young Scientists (no. BK20130012), the 333 Project Foundation of Jiangsu Province, the PAPD of Jiangsu Higher Education Institutions, and the Fundamental Research Funds for the Central Universities for financial support.

Supporting Information Available: XPS measurements of ensemble GQDs in the aging process and time-resolved measurements of ensemble GQDs excited with variable laser repetition rates. This material is available free of charge *via* the Internet at http://pubs.acs.org.

REFERENCES AND NOTES

1. Loh, K. P.; Bao, Q.; Eda, G.; Chhowalla, M. Graphene Oxide as a Chemically Tunable Platform for Optical Applications. *Nat. Chem.* **2010**, *2*, 1015–1024.
2. Eda, G.; Chhowalla, M. Chemically Derived Graphene Oxide: Towards Large-Area-Thin-Film Electronics and Optoelectronics. *Adv. Mater.* **2010**, *22*, 2392–2415.
3. Geim, A. K. Graphene: Status and Prospects. *Science* **2009**, *324*, 1530–1534.
4. Yeh, T.-F.; Chan, F.-F.; Hsieh, C.-T.; Teng, H. Graphite Oxide with Different Oxygenated Levels for Hydrogen and Oxygen Production from Water under Illumination: The Band Positions of Graphite Oxide. *J. Phys. Chem. C* **2011**, *115*, 22587–22597.
5. Wang, X.; Zhi, L.; Müllen, K. Transparent, Conductive Graphene Electrodes for Dye-Sensitized Solar Cells. *Nano Lett.* **2008**, *8*, 323–327.
6. Wu, J.; Agrawal, M.; Becerril, H. A.; Bao, Z.; Liu, Z.; Chen, Y.; Peumans, P. Organic Light-Emitting Diodes on Solution-Processed Graphene Transparent Electrodes. *ACS Nano* **2009**, *4*, 43–48.
7. Sun, X.; Liu, Z.; Welsher, K.; Robinson, J. T.; Goodwin, A.; Zaric, S.; Dai, H. Nano-Graphene Oxide for Cellular Imaging and Drug Delivery. *Nano Res.* **2008**, *1*, 203–212.
8. Gokus, T.; Nair, R. R.; Bonetti, A.; Böhmler, M.; Lombardo, A.; Novoselov, K. S.; Geim, A. K.; Ferrari, A. C.; Hartschuh, A. Making Graphene Luminescent by Oxygen Plasma Treatment. *ACS Nano* **2009**, *3*, 3963–3968.
9. Eda, G.; Lin, Y.-Y.; Mattevi, C.; Yamaguchi, H.; Chen, H.-A.; Chen, I.-S.; Chen, C.-W.; Chhowalla, M. Blue Photoluminescence from Chemically Derived Graphene Oxide. *Adv. Mater.* **2010**, *22*, 505–509.
10. Luo, Z.; Vora, P. M.; Mele, E. J.; Johnson, A. T.; Kikkawa, J. M. Photoluminescence and Band Gap Modulation in Graphene Oxide. *Appl. Phys. Lett.* **2009**, *94*, 111909.
11. Chien, C.-T.; Li, S.-S.; Lai, W.-J.; Yeh, Y.-C.; Chen, H.-A.; Chen, I.-S.; Chen, L.-C.; Chen, K.-H.; Nemoto, T.; Isoda, S.; *et al.* Tunable Photoluminescence from Graphene Oxide. *Angew. Chem., Int. Ed.* **2012**, *51*, 6662–6666.
12. Galande, C.; Mohite, A. D.; Naumov, A. V.; Gao, W.; Ci, L.; Ajayan, A.; Ajayan, P. M. Quasi-Molecular Fluorescence from Graphene Oxide. *Sci. Rep.* **2011**, *1*, 85.
13. Shang, J.; Ma, L.; Li, J.; Ai, W.; Yu, T.; Gurzadyan, G. G. The Origin of Fluorescence from Graphene Oxide. *Sci. Rep.* **2012**, *2*, 792.
14. Mei, Q.; Zhang, K.; Guan, G.; Liu, B.; Wang, S.; Zhang, Z. Highly Efficient Photoluminescent Graphene Oxide with Tunable Surface Properties. *Chem. Commun.* **2010**, *46*, 7319–7321.
15. Zhang, Z.; Zhang, J.; Chen, N.; Qu, L. Graphene Quantum Dots: An Emerging Material for the Energy-Related Applications and Beyond. *Energy Environ. Sci.* **2012**, *5*, 8869–8890.
16. Pan, D.; Zhang, J.; Li, Z.; Wu, M. Hydrothermal Route for Cutting Graphene Sheets into Blue Luminescent Graphene Quantum Dots. *Adv. Mater.* **2010**, *22*, 734–738.
17. Lu, J.; Yeo, P. S. E.; Gan, C. K.; Wu, P.; Loh, K. P. Transforming C60 Molecules into Graphene Quantum Dots. *Nat. Nanotechnol.* **2011**, *6*, 247–252.
18. Li, Y.; Hu, Y.; Zhao, Y.; Shi, G.; Deng, L.; Hou, Y.; Qu, L. An Electrochemical Avenue to Green-Luminescent Graphene Quantum Dots as Potential Electron-Acceptors for Photovoltaics. *Adv. Mater.* **2011**, *23*, 776–780.
19. Yan, X.; Cui, X.; Li, L. S. Synthesis of Large, Stable Colloidal Graphene Quantum Dots with Tunable Size. *J. Am. Chem. Soc.* **2010**, *132*, 5944–5945.
20. Peng, J.; Gao, W.; Gupta, B. K.; Liu, Z.; Romero-Aburto, R.; Ge, L.; Ajayan, P. M. Graphene Quantum Dots Derived from Carbon Fibers. *Nano Lett.* **2012**, *12*, 844–849.
21. Tang, L.; Ji, R.; Cao, X.; Lin, J.; Jiang, H.; Li, X.; Teng, K. S.; Luk, C. M.; Zeng, S.; Hao, J.; *et al.* Deep Ultraviolet Photoluminescence of Water-Soluble Self-Passivated Graphene Quantum Dots. *ACS Nano* **2012**, *6*, 5102–5110.
22. Jin, S. H.; Kim, D. H.; Jun, G. H.; Hong, S. H.; Jeon, S. Tuning the Photoluminescence of Graphene Quantum Dots through the Charge Transfer Effect of Functional Groups. *ACS Nano* **2013**, *7*, 1239–1245.
23. Liu, R.; Wu, D.; Feng, X.; Müllen, K. Bottom-Up Fabrication of Photoluminescent Graphene Quantum Dots with Uniform Morphology. *J. Am. Chem. Soc.* **2011**, *133*, 15221–15223.
24. Zhu, S.; Zhang, J.; Tang, S.; Qiao, C.; Wang, L.; Wang, H.; Liu, X.; Li, B.; Li, Y.; Yu, W.; *et al.* Surface Chemistry Routes to Modulate the Photoluminescence of Graphene Quantum Dots: From Fluorescence Mechanism to Up-Conversion Bioimaging Applications. *Adv. Funct. Mater.* **2012**, *22*, 4732–4740.
25. Kim, S.; Hwang, S. W.; Kim, M.-K.; Shin, D. Y.; Shin, D. H.; Kim, C. O.; Yang, S. B.; Park, J. H.; Hwang, E.; Choi, S.-H.; *et al.* Anomalous Behaviors of Visible Luminescence from Graphene Quantum Dots: Interplay between Size and Shape. *ACS Nano* **2012**, *6*, 8203–8208.
26. Gupta, V.; Chaudhary, N.; Srivastava, R.; Sharma, G. D.; Bhardwaj, R.; Chand, S. Luminscent Graphene Quantum Dots for Organic Photovoltaic Devices. *J. Am. Chem. Soc.* **2011**, *133*, 9960–9963.

27. Shen, J.; Zhu, Y.; Chen, C.; Yang, X.; Li, C. Facile Preparation and Upconversion Luminescence of Graphene Quantum Dots. *Chem. Commun.* **2011**, *47*, 2580–2582.
28. Li, L.; Wu, G.; Yang, G.; Peng, J.; Zhao, J.; Zhu, J.-J. Focusing on Luminescent Graphene Quantum Dots: Current Status and Future Perspectives. *Nanoscale* **2013**, *5*, 4015–4039.
29. Lakowicz, J. R. *Principles of Fluorescence Spectroscoy*, 2nd ed.; Plenum: New York, 1999.
30. Rogach, A. L.; Klar, T. A.; Lupton, J. M.; Meijerink, A.; Feldmann, J. Energy Transfer with Semiconductor Nanocrystals. *J. Mater. Chem.* **2009**, *19*, 1208–1221.
31. Hoheisel, W.; Colvin, V. L.; Johnson, C. S.; Alivisatos, A. P. Threshold for Quasicontinuum Absorption and Reduced Luminescence Efficiency in CdSe Nanocrystals. *J. Chem. Phys.* **1994**, *101*, 8455–8460.
32. Knappenberger, K. L., Jr.; Wong, D. B.; Xu, W.; Schwartzberg, A. M.; Wolcott, A.; Zhang, J. Z.; Leone, S. R. Excitation-Wavelength Dependence of Fluorescence Intermittency in CdSe Nanorods. *ACS Nano* **2008**, *2*, 2143–2153.
33. McGuire, J. A.; Sykora, M.; Joo, J.; Pietryga, J. M.; Klimov, V. I. Apparent *Versus* True Carrier Multiplication Yields in Semiconductor Nanocrystals. *Nano Lett.* **2010**, *10*, 2049–2057.
34. Pan, D.; Guo, L.; Zhang, J.; Xi, C.; Xue, Q.; Huang, H.; Wu, M. Cutting sp2 Clusters in Graphene Sheets into Colloidal Graphene Quantum Dots with Strong Green Fluorescence. *J. Mater. Chem.* **2012**, *22*, 3314–3318.
35. Yang, L.; Peng, H.; Huang, K.; Mague, T. J.; Li, H.; Lu, Y. Hierarchical Assembly of Organic/Inorganic Building Molecules with π-π Interactions. *Adv. Funct. Mater.* **2008**, *18*, 1526–1535.
36. Michler, P.; Kiraz, A.; Becher, C.; Schoenfeld, W. V.; Petroff, P. M.; Zhang, L.; Imamoglu, A. A Quantum Dot Single-Photon Turnstile Device. *Science* **2000**, *290*, 2282–2285.
37. Wang, X.; Ren, X.; Kahen, K.; Hahn, M. A.; Rajeswaran, M.; Maccagnano-Zacher, S.; Silcox, J.; Cragg, G. E.; Efros, A. L.; Krauss, T. D. Non-Blinking Semiconductor Nanocrystals. *Nature* **2009**, *459*, 686–689.
38. Empedocles, S. A.; Neuhauser, R.; Shimizu, K.; Bawendi, M. G. Photoluminescence from Single Semiconductor Nanostructures. *Adv. Mater.* **1999**, *11*, 1243–1256.
39. Frantsuzov, P.; Kuno, M.; Janko, B.; Marcus, R. A. Universal Emission Intermittency in Quantum Dots, Nanorods and Nanowires. *Nat. Phys.* **2008**, *4*, 519–522.
40. Ishigami, M.; Chen, J. H.; Cullen, W. G.; Fuhrer, M. S.; Williams, E. D. Atomic Structure of Graphene on SiO_2. *Nano Lett.* **2007**, *7*, 1643–1648.
41. Paredes, J. I.; Villar-Rodil, S.; Solís-Fernández, P.; Martínez-Alonso, A.; Tascón, J. M. D. Atomic Force and Scanning Tunneling Microscopy Imaging of Graphene Nanosheets Derived From Graphite Oxide. *Langmuir* **2009**, *25*, 5957–5968.
42. Gómez-Navarro, C.; Meyer, J. C.; Sundaram, R. S.; Chuvilin, A.; Kurasch, S.; Burghard, M.; Kern, K.; Kaiser, U. Atomic Structure of Reduced Graphene Oxide. *Nano Lett.* **2010**, *10*, 1144–1148.